Large-eddy simulations of flow and heat transfer around a low-Mach number turbine blade

By N. Maheu†, V. Moureau†, P. Domingo†, F. Duchaine‡ and G. Balarac¶

Modeling of wall bounded flows and conjugate heat transfer (CHT) is known to be a challenging task for Large-Eddy Simulation (LES). In the boundary layers, the inertial and dissipative scales have similar sizes, which implies relying on different modeling approaches than those used in free turbulent flows. To this aim, a numerical database of highly-refined LES and CHT simulations is built and used to validate a novel tabulated wall model based on the work of Duprat *et al.* (2011).

1. Introduction

In recent decades, the compression ratio in aeronautical gas turbines has increased steadily. In the ideal Brayton cycle, an increase of the pressure ratio directly leads to an increase of the thermodynamic efficiency and subsequently to a decrease of the specific fuel consumption. Unfortunately, this pressure ratio growth causes a direct increase of the temperature ratio through the turbine stages, which may impact the design of turbine blades. Large-Eddy Simulation (LES) is a promising tool for the prediction of heat transfer on turbine blades (Bhaskaran & Lele 2011). However, wall treatment in LES is a well-known issue mainly related to the high resolution required to capture near-wall phenomena. Several strategies have been proposed to tackle this issue. In the thin-boundary layer (TBL) model (Balaras *et al.* 1996) or in detached-eddy simulations (DES) (Spalart *et al.* 1997), a different set of equations is solved in the near-wall region. Another solution is to impose the viscous and thermal fluxes at the wall assuming that velocity and temperature in the near-wall region follow the law-of-the-wall. As the model choice may have a dramatic influence on local pressure losses and heat transfer, improvements are still needed to achieve a better reliability of the closures. In the first part of the paper, a numerical database of highly-refined wall-resolved LES and conjugate heat transfer simulations is presented. In the second part, a tabulated wall model, which takes into account the effect of the pressure gradient, is derived and validated.

2. A numerical database for model verification

2.1. *Highly-refined wall-resolved LES*

In order to gain insight into the flow physics of heat transfer in turbine blades, highly-refined simulations of a low-Mach number turbine blade are carried out with the YALES2 solver (Moureau *et al.* 2011*b*,*a*) developed at CORIA.

† CORIA, CNRS UMR6614, Universite et INSA de Rouen, Saint-Etienne du Rouvray, France
‡ CERFACS, 41 avenue Coriolis, Toulouse, France
¶ LEGI, CNRS UMR5519, Universite Joseph Fourier et Institut National Polytechnique de Grenoble, Grenoble, France

Mesh	Cell count	Min. cell size (μm)	Max. y^+	Number of flow-through times
M0	1M	120	88	19.5
M1	35M	30	24	33.9
M2	280M	15	20	11.1
M3	2.2B	7.5	14	3.3
M4	17.9B	3.75	4	0.9
M5	143B	1.9	-	(60 iterations)

TABLE 1. Description of the computational database

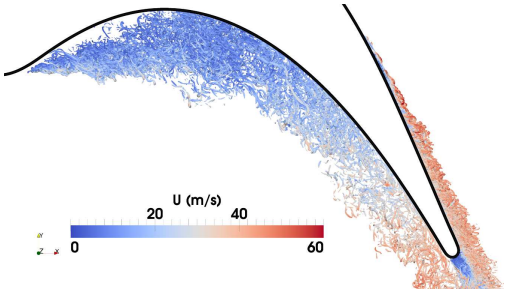

FIGURE 1. Turbulent structures around the blade with the M4 mesh.

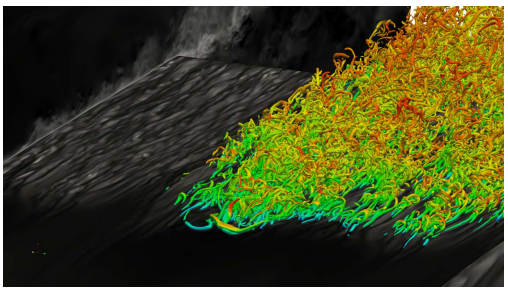

FIGURE 2. Effect of near wall structures on heat transfers at the trailing edge of the suction side.

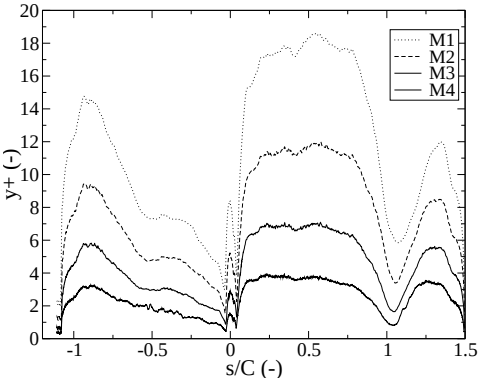

FIGURE 3. Evolution of y^+ on the different meshes.

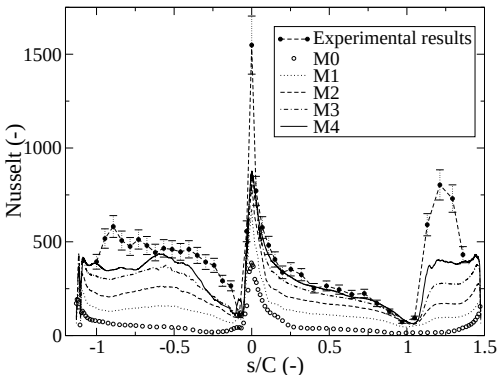

FIGURE 4. Evolution of the Nusselt number based on the resolved gradient.

2.1.1. *Numerical setup*

The blade, which is immersed in a hot turbulent flow, is internally liquid cooled in order to maintain a nearly constant wall temperature. The coolant flows in ten cylindrical holes of various diameters. The chosen turbine blade design based on a 2D profile extruded in the spanwise direction is typical of a cooled low-pressure turbine blade with moderate to nearly high loading. The intent of the design was to generate a large flow separation zone on the blade pressure side and a transition of the boundary layer from laminar to

turbulent on the suction side. A detailed experimental investigation of this blade cascade was conducted by Ladisch *et al.* (2009). Measurements were achieved in an atmospheric linear cascade facility, which allowed for a variation of the free-stream Reynolds number and turbulence intensity. In the present work, the Reynolds number based on the chord length C is 150,000 with a turbulence injection rate of 6%. Upstream turbulence is known to have an important effect on the pressure and heat transfer distributions (Bhaskaran & Lele 2011). The computational domain is approximately $3C$ long in the streamwise direction and $C/3$ long in the spanwise direction. The simulation database consists of LES with increasing resolutions that are summarized in Table 1. All the calculations of the section are performed with a variable-density fractional-step method for low-Mach number flows and a localized dynamic Smagorinsky model (Germano *et al.* 1991). All the meshes are tetrahedron-based. This element type allows to refine the mesh close to the wall while ensuring a good cell size isotropy to capture the smallest vortices accurately. The mesh M4 reaches a high resolution at the wall as illustrated in Figures 1 and 2, where coherent structures are highlighted by iso-contours of Q-criterion. In Figure 2, the Nusselt number on the blade surface is also represented to stress the link between the vortices and the local heat transfer. To assess the resolution of the computations, the dimensionless wall distance y^+ of the first cell at the wall is represented in Figure 3 as a function of the normalized curvilinear abscissa s/C. This abscissa is positive on the suction side, negative on the pressure side and zero at the stagnation point.

2.1.2. *Mesh convergence of heat transfer*

The mesh convergence is assessed investigating a Nusselt number based on the resolved temperature gradient. This Nusselt number plotted in Figure 4 is computed from the values provided by the resolution of the LES equations at the first control volume in the fluid: $Nu_{grad} = (\nabla \widetilde{T})C/(T_\infty - T_w)$, where $\widetilde{T}$, T_∞ and T_w are the resolved, upstream and wall temperatures, respectively. This Nusselt number does not take into account the sub-grid scale heat flux and is mainly used as a resolution indicator. In Figure 4, the evolution for the five levels of mesh refinement can be seen. For the two finest meshes, the temperature gradient is sufficiently resolved to capture the heat transfer in most areas: in the laminar and turbulent layers on the suction side with the correct position of the transition at $s/C = 1.1$ and in the recirculation zone on the pressure side. However, at the stagnation point, where the strongest gradient is met, even if the y^+ is small, the experimental value of the Nusselt number is not recovered. To try to explain this discrepancy, conjugate heat transfer calculations and an uncertainty quantification analysis are performed for this particular blade.

2.2. *Investigation of conjugate heat transfers*

To complete the wall-resolved LES database, conjugate heat transfer (CHT) simulations of the same blade are performed with the thermal solver AVTP developed by CERFACS and with the LES flow solvers AVBP (Schønfeld & Rudgyard 1999) jointly developed by CERFACS and IFP-EN, and YALES2. The exit Reynolds number is the same as the one of the previous section but no turbulence is injected to avoid dealing with some compressibility issues (Collado *et al.* 2012). Since both flow solvers give very similar results, only results obtained with AVBP are presented in this section.

2.2.1. *Numerical setup*

For the CHT simulations, a hybrid approach with five prismatic layers in the near-wall region, Figure 5, is adopted to reduce the number of cells and to meet the preferential

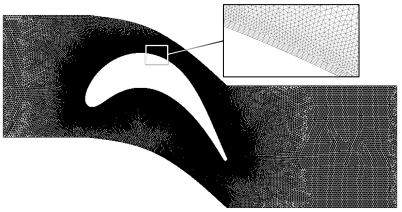

FIGURE 5. Detail of the unstructured mesh grid of the fluid domain used for CHT.

Mesh	H1	H2	H3	H4
Δy (μm)	62.5	50	25	12.5
mean y^+	5.7	4.6	2.5	1.3
$\Delta x/\Delta y$	4	4	4	8
# nodes	1.8 M	2.5 M	7.3 M	10.3 M
# cells	9.3 M	13.2 M	37.4 M	54.8 M
# prisms	0.3 M	0.5 M	2.2 M	2.2 M
# wall nodes	35 K	55 K	220 K	220 K
Time step	67.6 ns	54.9 ns	26.7 ns	20.0 ns

TABLE 2. Properties of the meshes used for the fluid.

directions of the boundary layer flow. A convergence study of the wall friction and wall heat flux depending on the height of the prisms at the wall Δy has been done based on four meshes detailed in Table 2. The aspect ratio of the prisms at the wall is less than 8 in agreement with known observations and boundary layer scales (Sagaut 2000). In the fluid, the σ sub-grid scale model (Nicoud *et al.* 2011) is used in conjunction with isothermal no-slip wall conditions. This model is designed to provide a correct turbulent viscosity scaling at the wall. NSCBC boundary conditions (Poinsot & Lele 1992; Granet *et al.* 2010) are used for the inlet and outlet of the domain.

2.2.2. *Mesh convergence with isothermal computations*

Figure 6 presents the evolution of the normalized wall distance y^+ around the blade for the four meshes. As all the simulations on the four meshes capture almost the same flow topology, the shapes of all y^+ profiles are similar. For the mesh H4, the maximum value of y^+ is always below 2 and the mean value around the blade is 1.3. In the other directions, the aspect ratio of the prisms gives suitable normalized wall distances x^+ and z^+ around 16 (Sagaut 2000). The heat transfer coefficient at the curvilinear abscissa s is defined by the ratio between the wall heat flux, q_w, and the difference between the upstream temperature T_∞ and the local wall temperature T_w: $h(s) = q_w(s)/(T_\infty - T_w(s))$. The mesh convergence of the heat transfer coefficient h is illustrated in Figure 7 with $T_w(s) =$ 300 K. The results from meshes H3 and H4 are almost super-imposed except at the leading edge as well as in the turbulent regions of both suction and pressure sides. With mesh H4, the prediction of the h is very close to the experimental measurement on a large part of the blade wall. The largest discrepancy is located at the leading edge similarly to the calculations in the previous section. Heat transfer is also underestimated near the trailing edge on the suction side where the boundary layer reattaches as well as on the pressure side where the large separation takes place.

2.2.3. *CHT results*

The airfoils material is a titanium alloy with a thermal conductivity $\lambda_s \approx 7\ \mathrm{W\cdot m^{-1}\cdot K^{-1}}$ and a density $\rho_s = 4420\ \mathrm{kg\cdot m^{-3}}$. Both the conductivity and the heat capacity are fitted with second-order polynomials law:

$$\lambda_s = 3.2288 + 0.0091T + 7\ 10^{-6}T^2\ (\mathrm{W\cdot m^{-1}\cdot K^{-1}})\,, \tag{2.1}$$

$$C = -80.131 + 2.8794T - 0.003085T^2\ \mathrm{J\cdot K^{-1}}\,. \tag{2.2}$$

The solid blade is meshed with 1.8M tetrahedral cells and 360 567 nodes with a characteristic size of 0.2 mm on the fluid/solid interface as well as close to the cooling holes

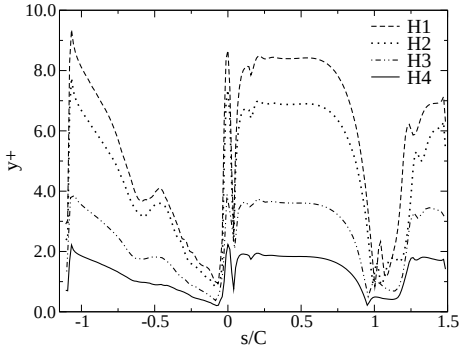

FIGURE 6. y^+ distribution along the blade profile for the four meshes.

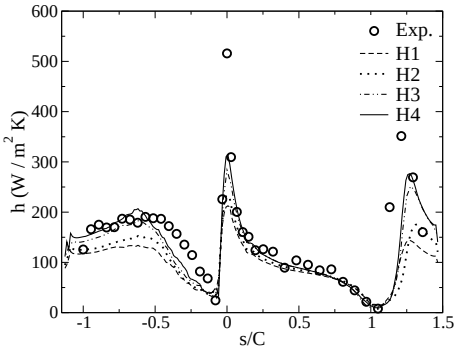

FIGURE 7. Heat transfer coefficient h distribution along the blade profile.

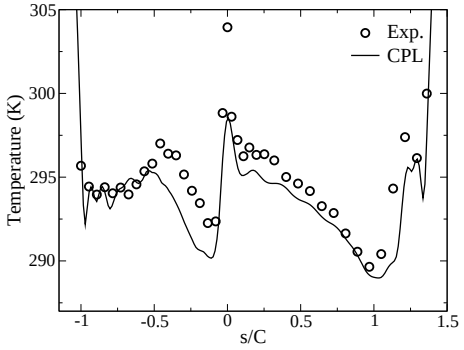

(a)

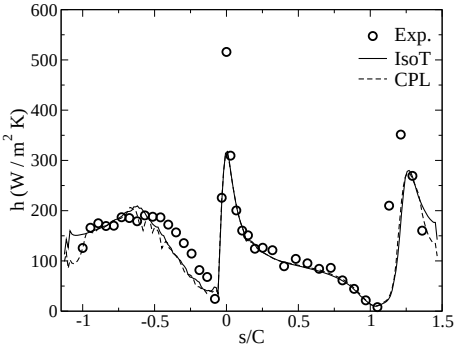

(b)

FIGURE 8. (a) Temperature distribution around the blade obtained by CHT and (b) h obtained with an isothermal computation (IsoT) and the coupled simulation (CPL) for the mesh H4.

and with a characteristic size of 1 mm elsewhere. Convective conditions are imposed in the ten cooling holes inside the blade with convective temperatures and heat transfer coefficients provided by experimentalists. The wall heat flux computed by the fluid solver is imposed as a boundary condition to the solid part and the temperature of the solid surface is given back to the fluid wall. To avoid simulating the whole transient temperature evolution of the solid temperature, the asynchronized coupling approach proposed by citeDuchaine:2009b is used. To ensure the stability of this coupling, information at the fluid/solid interface is exchanged with a very high frequency (Giles 1997; Duchaine *et al.* 2009), i.e. at every iteration of the thermal solver AVTP and after ten iterations of the fluid solver. In terms of physical time, the solid boundary conditions are updated each 20 ms while the surface temperature of the fluid is updated every 200 ns.

Figure 8(a) presents the temperature distribution around the blade. The CHT results are in very good agreement with the experimental temperature profile both in terms of levels and shape. The underestimates of convective heat transfer previously underlined lead to under-predictions of the temperature levels at the leading edge and seem to have an influence at the beginning of the suction side. Temperature underestimates also occur in the large recirculation zone on the pressure side and in the transition region of the suction side. The convective heat transfer coefficients from the isothermal computation

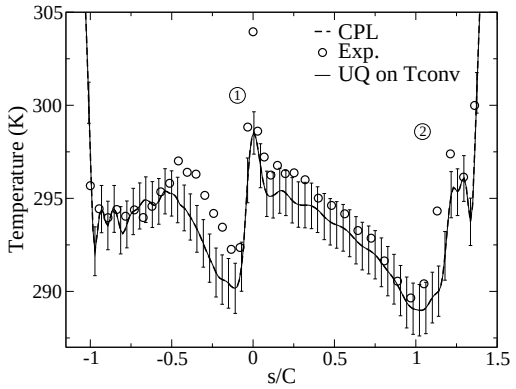

FIGURE 9. Mean and 95% confident interval of the temperature distribution around the blade with respect to uncertainty in convective conditions in the holes.

and the coupled simulation are compared with the experimental ones in Figure 8(b). In the coupled case, h is obtained from the local wall temperature T_w given in Figure 8(a). The results from the two simulations are superimposed on a large part of the profile. The main difference is at the trailing edge on both suction and pressure sides where the coupled results improve the prediction of the heat transfer coefficient. The assumption of constant temperature at 300K to extract the convective coefficient is wrong in this region while having the right temperature allows predicting the correct heat flux.

2.2.4. *Uncertainty quantification of the temperature predictions*

The CHT simulation gives accurate distribution of heat transfer coefficient and temperature on the blade. It is then interesting to check the dependence of the distributions to uncertain input parameters of the cooling system. Uncertainty quantification of the blade temperature distribution to the temperature inside the cooling holes is reported here. The experimental uncertainty on this cooling temperature is about 0.85%. The sampling method used here is based on the stochastic collocation with Clenshaw-Curtis quadrature points with the same weights for each hole. To obtain the desired statistics, the output temperature function is built from the sampling using Lagrange polynomials. The convergence of the temperature mean and standard deviation is obtained with only 3 Clenshaw-Curtis quadrature points. Figure 9 presents the mean and 95% confidence interval of the temperature distribution resulting from the uncertainty quantification. The temperature profile is largely affected by the knowledge of the cooling temperature: the standard deviation ranges from 0.7 K near the trailing edge to 1.4K close to the leading edge and in the separation zone on the suction side, with an average value of about 1.23 K. Experimental measurements are included in the simulation error bars in most parts of the profile except at the leading edge ① and in the recirculation zone on the pressure side ②, where the discrepancies in the highly-refined LES database were observed.

3. A tabulated law-of-the-wall model

3.1. *Description of the wall model*

Wall models have to take into account the complexity of the flow physics in the boundary layer. In particular, models have to represent the effect of the adverse pressure gradient, which ultimately leads to transition, or the separation and reattachment zones on the

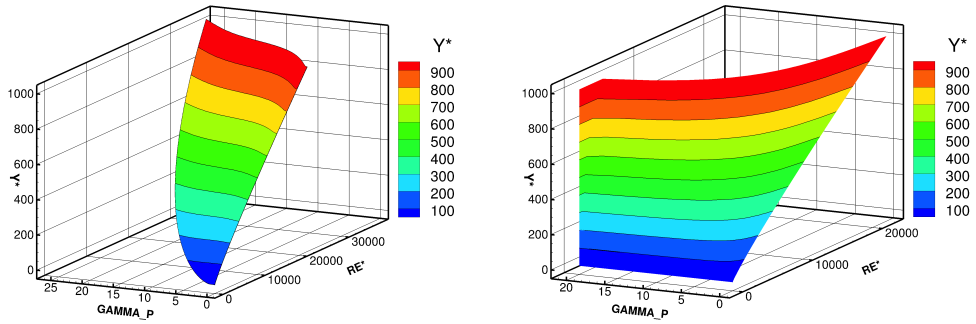

FIGURE 10. Non-dimensionalized wall distance $y^\star$ as a function of $Re^\star$ and $\gamma_p^\star$ for a favorable pressure gradient (left) and for an adverse pressure gradient (right).

pressure side. To this aim, Duprat *et al.* (2011) developed a model, which takes into account the local tangential pressure gradient. Compared to conventional law-of-the-wall derivations, where the pressure gradient is neglected, Duprat *et al.* keep the pressure gradient term in the momentum equation and propose a turbulent viscosity scaling, which is dependent on the normalized wall distance, and a parameter α related to the streamwise pressure gradient. This parameter is defined from the wall friction velocity u_τ, the pressure gradient velocity u_p (Simpson 1983) and the mixed friction velocity $u_{\tau p}$,

$$\tau_w = \rho\nu\frac{\partial\overline{u}}{\partial y}\bigg|_w\,,\quad u_\tau = \sqrt{|\tau_w|/\rho}\,,\quad u_p = \left|\frac{\nu}{\rho}\frac{\partial\overline{P}}{\partial x}\right|^{1/3}\,,\quad u_{\tau p} = \sqrt{u_\tau^2+u_p^2}\,,\quad \alpha = \frac{u_\tau^2}{u_{\tau p}^2}\,, \tag{3.1}$$

where τ_w, ρ, ν, $\overline{P}$ are the wall shear stress, the density, the kinematic viscosity and the pressure, respectively. From these parameters, the turbulent viscosity scaling reads

$$\frac{\nu_t}{\nu} = \kappa y^\star[\alpha+y^\star(1-\alpha)^{\frac{3}{2}}]^\beta\left[1-\exp\left(\frac{-y^\star}{1+A\alpha^3}\right)\right]^2\,,\ \text{where } y^\star = \frac{yu_{\tau p}}{\nu}\,,\ \overline{u}^\star = \frac{\overline{u}}{u_{\tau p}}\,. \tag{3.2}$$

κ is the Kàrmàn constant and A is a model constant. Then, the normalized velocity gradient reads

$$\frac{\partial\overline{u}^\star}{\partial y^\star} = \frac{s_p(1-\alpha)^{\frac{3}{2}}y^\star+s_\tau\alpha}{1+\nu_t/\nu}\,,\ \text{where } s_p = \text{sign}(\partial\overline{P}/\partial x)\,,\quad s_\tau = \text{sign}(\tau_w)\,. \tag{3.3}$$

The normalized temperature is obtained from the temperature difference between the flow and the wall divided by the temperature gradient at the wall, and the normalized temperature gradient is derived similarly to the velocity gradient:

$$\frac{\overline{T}^\star}{y^\star} = \frac{\overline{T}-T_w}{y}\left.\frac{\partial\overline{T}}{\partial y}\right|_w^{-1}\ \text{and}\ \frac{\partial\overline{T}^\star}{\partial y^\star} = \frac{1}{1+(Pr/Pr_t)(\nu_t/\nu)}\,. \tag{3.4}$$

To close the model, an additional correlation for the turbulent Prandtl number is assumed (Kays 1994): $Pr_t = 0.85+2\nu/(\nu_t Pr)$. In this model, the gradients of the normalized velocity $\overline{u}^\star$ and temperature $\overline{T}^\star$ are explicit functions of $y^\star$ and α, and the profiles of normalized velocity and temperature are found by integrating the gradient along the wall normal direction. The main issue is that the wall shear stress and heat flux cannot be directly computed from the resolved variables of the LES. A Newton-Raphson algorithm is required to find a set of variables $y^\star$ and α that match the resolved velocity and temperature at the first control volume in the fluid. To overcome this issue, a tabulation

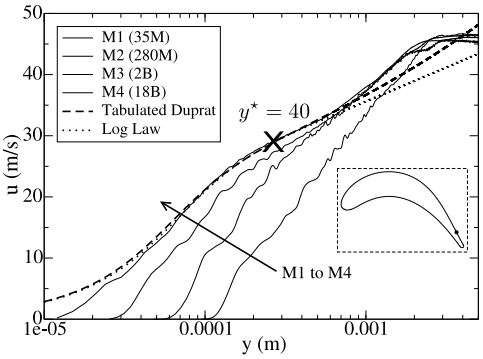

FIGURE 11. Velocity profiles at $s/C = 1.35$ on the suction side.

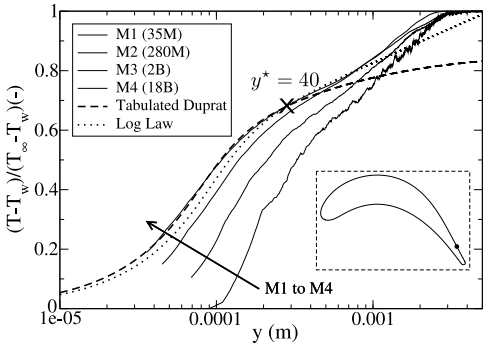

FIGURE 12. Temperature profiles at $s/C = 1.35$ on the suction side.

technique is proposed. This type of methodology is widely used in the combustion field, where low-dimensional manifolds with a few control variables may be used to describe the state of a chemical system. In order to apply this approach to the present wall model, two control parameters based on the resolved LES variables are necessary. After several numerical tests, two parameters $Re^\star$ and $\gamma_p^\star$ have been chosen

$$Re^\star = \frac{\overline{u}y}{\nu} = \overline{u}^\star y^\star \,, \quad \gamma_p^\star = \frac{u_p^2}{\overline{u}^2 + u_p^2} Re^\star = \frac{1-\alpha}{(\overline{u}^\star)^2 + (1-\alpha)} \overline{u}^\star y^\star \,. \tag{3.5}$$

The parameter $Re^\star$ is a Reynolds number based on the resolved variables at the first control volume in the fluid and $\gamma_p^\star$ is closely related to α. Both parameters may be computed directly from the resolved variables in the LES. The final model is obtained by tabulating the normalized distance $y^\star$ and a Nusselt number $Nu^\star = y^\star/\overline{T}^\star$ as functions of $Re^\star$ and $\gamma_p^\star$. The dependence of $y^\star$ on these parameters is illustrated in Figure 10.

3.2. *A priori validation of the wall model*

The tabulated Duprat model (TDM) has been first validated a priori with the database of highly refined LES presented in the first section of the report. The validation is performed there by comparing the velocity and temperature profiles given by the analytical model to the database of wall-resolved LES with different resolutions. Figures 11 and 12 show the velocity and temperature profiles close to the trailing edge on the suction side ($s/C = 1.35$). The comparison is done by choosing a value of $y^\star$ and then, from the values that are tabulated, by plotting the entire velocity and temperature profiles predicted by the present model and by a classical log law. For the velocity profiles, it can be observed that the two models give a reasonable agreement with the finest mesh resolution and the TDM gives a better estimate of the velocity profile in the outer layer. For the temperature profiles, the agreement is slightly better with the TDM than with the log law.

3.3. *A posteriori validation of the wall model*

To further validate the model, coarse no-slip and wall-modeled LES are performed with three types of boundary treatment: no-slip boundary condition, log law and tabulated Duprat model. The mesh chosen for this validation is the mesh M1. First, to validate the aerodynamics, the pressure profiles obtained with the three models are compared to the results of the database with the M4 mesh and to the experiments. The results are shown in Figure 13. It can be noticed that the results are in good agreement for the

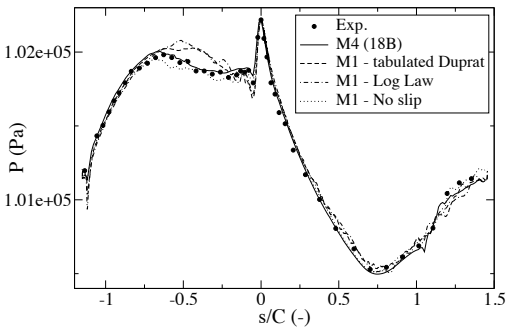

FIGURE 13. Pressure distribution obtained in the different wall-modeled LES.

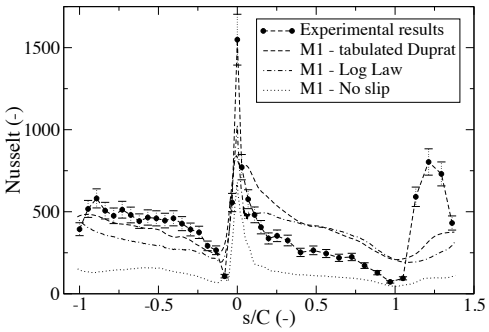

FIGURE 14. Nusselt number obtained in the different wall-modeled LES.

three cases reproducing the main features of the flow. Wall-modeled LES exhibit a slight discrepancy in the recirculation bubble on the pressure side compared to the no-slip boundary treatment. Then, the Nusselt number is compared in Figure 14. Compared to the no-slip boundary condition, which largely underestimates the Nusselt number when based on the resolved temperature gradient, the wall-modeled LES are more accurate and they feature an inflection on the suction side, where the transition occurs. More particularly, the TDM correctly predicts the heat exchanges on the pressure side. The two wall models have some difficulties capturing the laminar boundary layer with an adverse pressure gradient on the suction side. This point has to be further investigated.

4. Conclusions

A numerical database of highly-refined wall-resolved LES has been built and used to compare wall models for the prediction of heat transfer. To complement this database and better understand the discrepancies between the simulations and the experiments, LES coupled with a thermal solver have been carried out. An uncertainty quantification analysis showed that most of the discrepancies may be explained by the cooling temperature uncertainty except at the leading and trailing edges. This comprehensive database was then used to a priori and a posteriori validate a tabulated wall model for wall friction and heat flux, which takes into account the pressure gradient. This tabulated model offers interesting perspectives as it may be enriched with additional control parameters to include more effects such as roughness. The look-up tables could also be constructed from the highly-refined LES instead of analytic laws in order to improve the predictions.

Acknowledgments

The results in this report have been achieved using the PRACE Research Infrastructure resource Curie based in France at the CEA-TGCC center under the allocation x2012026880. This work was also granted access to the HPC resources of IDRIS under the allocation 2012-6880 made by GENCI. The authors would like to gratefully thank their CTR hosts Ivan Bermejo-Moreno and Julien Bodart, and Stéphane Moreau from Sherbrooke University.

REFERENCES

Balaras, E., Benocci, C. & Piomelli, U. 1996 Two-layer approximate boundary conditions for large-eddy simulations. *AIAA J.* **34** (6), 1111–1119.

Bhaskaran, R. & Lele, S. K. 2011 Heat Transfer Prediction in High Pressure Turbine Cascade with Free-Stream Turbulence using LES. In *41st AIAA Fluid Dynamics Conference and Exhibit, AIAA 2011-3266*.

Collado, E., Gourdain, N., Duchaine, F. & Gicquel, L. 2012 Effects of free-stream turbulence on high pressure turbine blade heat transfer predicted by structured and unstructured LES. *Int. J. Heat and Mass Transfer* **55** (21-22), 5754–5768.

Duchaine, F., Corpron, A., Pons, L., Moureau, V., Nicoud, F. & Poinsot, T. 2009 Development and assessment of a coupled strategy for conjugate heat transfer with Large Eddy Simulation. application to a cooled turbine blade. *Int. J. of Heat and Fluid Flow* **30** (6), Pages 1129–1141.

Duprat, C., Balarac, G., Métais, O., Congedo, P. M. & Brugière, O. 2011 A wall-layer model for large-eddy simulations of turbulent flows with/out pressure gradient. *Phys. Fluids A: Fluid Dynamics* **23**, 015101.

Germano, M., Piomelli, U., Moin, P. & Cabot, W. H. 1991 A dynamic subgrid-scale eddy viscosity model. *Phys. Fluids* **3** (7), 1760–1765.

Giles, M. 1997 Stability analysis of numerical interface conditions in fluid-structure thermal analysis. *Int. J. Numer. Meth. Fluids* **25** (4), 421–436.

Granet, V., Vermorel, O., Leonard, T., Gicquel, L., & Poinsot, T. 2010 Comparison of nonreflecting outlet boundary conditions for compressible solvers on unstructured grids. *AIAA Journal* **48** (10), 2348–2364.

Kays, W. 1994 Turbulent Prandtl number. Where are we? *ASME Transactions Journal of Heat Transfer* **116**, 284–295.

Ladisch, H., Schulz, A. & Bauer, H.-J. 2009 Heat transfer measurements on a turbine airfoil with pressure side separation. In *ASME Turbo Expo 2009 : Power for Land, Sea, and Air*. Orlando, Florida, USA.

Moureau, V., Domingo, P. & Vervisch, L. 2011*a* Design of a massively parallel CFD code for complex geometries. *Comptes Rendus Mécanique* (339), 141–148.

Moureau, V., Domingo, P. & Vervisch, L. 2011*b* From Large-Eddy Simulation to Direct Numerical Simulation of a lean premixed swirl flame: Filtered laminar flame-PDF modeling. *Comb. & Flame* **158** (7), 1340–1357.

Nicoud, F., Toda, H. B., Cabrit, O., Bose, S. & Lee, J. 2011 Using singular values to build a subgrid-scale model for large eddy simulations. *Physics of Fluids A: Fluid Dynamics* **23** (8), 085106.

Poinsot, T. & Lele, S. 1992 Boundary conditions for direct simulations of compressible viscous flows. *J. Comput. Phys.* **101** (1), 104–129.

Sagaut, P. 2000 *Large Eddy Simulation for incompressible flows*. Springer-Verlag.

Schønfeld, T. & Rudgyard, M. 1999 Steady and unsteady flows simulations using the hybrid flow solver avbp. *AIAA Journal* **37** (11), 1378–1385.

Simpson, R. L. 1983 A model for the backflow mean velocity profile. *AIAA journal* **21** (1), 142–143.

Spalart, P. R., Jou, W. H., Strelets, M. & Allmaras, S. R. 1997 Comments on the feasibility of les for wings and on the hybrid rans/les approach. In *Adv. in DNS/LES, 1st AFOSR Int. Conf. On DNS/LES*. Ruston, LA, USA.